A New Combined Differential-Discrete Cellular Automaton Approach for Biofilm Modeling: Application for Growth in Gel Beads

Cristian Picioreanu, Mark C. M. van Loosdrecht, Joseph J. Heijnen

Delft University of Technology, Department of Biochemical Engineering, Kluyver Laboratory for Biotechnology, Julianalaan 67, 2628 BC Delft, The Netherlands; telephone: +31 15 2781618; Fax: +31 15 2782355; e-mail: Mark.vL@stm.tudelft.nl

Received 25 March 1997; accepted 12 September 1997

Abstract: The theoretical basis and quantitative evaluation of a new approach for modeling biofilm growth are presented here. Soluble components (e.g., substrates) are represented in a continuous field, whereas discrete mapping is used for solid components (e.g., biomass). The spatial distribution of substrate is calculated by applying relaxation methods to the reaction–diffusion mass balance. A biomass density map is determined from direct integration in each grid cell of a substrate-limited growth equation. Spreading and distribution of biomass is modeled by a discrete cellular automaton algorithm. The ability of this model to represent diffusion–reaction–microbial growth systems was tested for a well-characterized system: immobilized cells growing in spherical gel beads. Good quantitative agreement with data for global oxygen consumption rate was found. The calculated concentration profiles of substrate and biomass in gel beads corresponded to those measured. Moreover, it was possible, using the discrete spreading algorithm, to predict the spatial two- and three-dimensional distribution of microorganisms in relation to, for example, substrate flux and inoculation density. The new technique looks promising for modeling diffusion–reaction–microbial growth processes in heterogeneous systems as they occur in biofilms. © 1998 John Wiley & Sons, Inc. *Biotechnol Bioeng* **57:** 718–731, 1998.

Keywords: biofilm; modeling; reaction–diffusion–growth; cellular automata; immobilized cells; structure

INTRODUCTION

There are now several mechanistic mathematical models that describe fairly well conversion of soluble substrates by biofilms and, with reasonable insight, population dynamics (Arvin and Harremoës, 1990; Characklis and Marshall, 1989; Wanner and Gujer, 1986; Wanner and Reichert, 1996). Both features can be well predicted provided the biofilm structure is known. With rare exceptions, all mathematical models treat the biofilm as a one-dimensional structure. However, structural heterogeneity, including non-uniform distribution of cells and polymers, variable biofilm thickness and surface shape, and variable density and porosity, has been proven and quantitatively measured by many researchers (Gjaltema et al., 1994; van Loosdrecht et al., 1995; Zhang and Bishop, 1994a, b). In the current biofilm models, biofilm density, porosity, and surface shape are to be specified as model input. No available model can predict these properties associated with biofilm heterogeneity. We believe that a combined discrete representation of the solid phase (e.g., by cellular automata, CA) with classical continuous methods for soluble components offers the possibility to predict the biofilm structure.

The geometrical structures of several biological communities have already been modeled by CA methods. For bacteria colonies, a diffusion-limited aggregation (DLA) model was used by Fujikawa (1994) and a different random-walk model was applied by Schindler and Rataj (1992) and Schindler and Rovensky (1994). All these models can produce complex growth patterns as observed on agar slabs (Matsushita and Fujikawa, 1990), but no explicit conversion of ''nutrients'' has been included. Biomass accumulation rate, mycelial density, and differentiation of filamentous fungi on solid surfaces have also been generated by a probabilistic CA (Laszlo and Silman, 1993). There is also a series of CA models for proliferation of animal cells (Hawboldt et al., 1994; Lim and Davies, 1990; Zygourakis et al., 1991). A more realistic representation of colony growth was made by Ben-Jacob et al. (1994) who included in their model the explicit growth of bacteria in a substrate gradient field. Both in this study and in that of Takács and Fleit (1995), who modeled the filamentous bulking of activated sludge, the nutrient field was solved by finite difference methods. The first mentioned application of CA modeling in biofilm research was in a recent study by Wimpenny and Colasanti (1997), based on ideas discussed earlier by Colasanti (1992). This model is, however, strongly comparable to the DLA models because growth is only considered at the surface (where unoccupied space is available) and hardly in-

Correspondence to: M. van Loosdrecht

Contract grant sponsor: The Netherlands Organization for Applied Scientific Research

Contract grant number: 95/638/MEP

CCC 0006-3592/98/060718-14

side the biofilm structure. A quite different approach was used in the model by Barker and Grimson (1993), in which both diffusion and reaction of substrates forming biomass are represented by CA algorithms.

However, we believe that, for a system scale of millimeters, only the solid particle dynamics (bacteria, polymers, carrier) must be modeled in a discrete way, whereas the nutrient field is solved by finite difference methods. This leads to a faster (and more realistic) model solution, affordable on a common personal computer.

A common drawback the aforementioned models is the use of abstract, mathematical parameters (''units of resource,'' ''random-walk distance,'' etc.), which are not explicitly linked to the macroscopic physical/chemical/biological parameters commonly used to describe biofilm systems (yields, concentrations, rates, fluxes of nutrients). Past models produce various patterns as a response to changing parameters, but they evolve in abstract time. By combining differential with discrete models, we can predict biofilm structure, together with correct time evolution of concentrations, fluxes, and conversion rates.

As far as we know, the model we describe in this work is the first quantitative validation of a biofilm model that includes CA rules. To validate this approach, we applied the model to a well-characterized system: the growth of immobilized cells in a gel matrix (Wijffels et al., 1991a). A good quantitative agreement with data for global oxygen consumption rate was found. The model-predicted concentration profiles of substrate and biomass in the gel beads also corresponded to those measured. Due to the ''discrete spreading'' algorithm for biomass, it is possible to correctly predict the spatial two-dimensional (2D) and three-dimensional (3D) distribution of microorganisms in relation to, for example, the substrate flux and inoculation density.

MODEL DEFINITION

The Space

The physical space is represented by a rectangular uniform grid. Either square elements are used as tiles to fill the 2D space or cubic volume elements are used to fill the 3D volume. In the $N \times M \times L$ 3D Cartesian grid, coordinates of volume elements are given by a vector $(x,y,z) \in (0 \ldots N-1, 0 \ldots M-1, 0 \ldots L-1)$.

The Variables

Two variables are chosen to represent the state of the system that simulates the biofilm development in the simplest case: the soluble limiting substrate concentration (S) and biomass density (C) (both in dimensionless form). In addition, we use a third matrix for ''solid components,'' called **c.** In this matrix we store information about the occupation state of space with solid particles (bacteria, gel, substratum, etc.).

The States

Each element, $S_{x,y,z}$, of the substrate matrix, **S,** will take *real* values between 0 and 1. The biomass content of each volume element (represented by matrix **C**) also varies in the same range. The occupation state of space (matrix **c**), takes the value of 0 for an unoccupied site (meaning liquid phase), 1 for occupied with biomass, and 2 for occupied with carrier (or gel in immobilized cells systems). One bacterial cell fills the whole elemental volume *only* when we work with large matrices (so that the grid size is small enough, as we will see later). Otherwise, when the size of a grid element is larger than the bacterial size, $c_{x,y,z} = 1$ means that the element is marked as containing biomass (no matter if there is a colony or only one cell).

The Rules

The matrices **S, C,** and **c** are updated according to different rules, corresponding to different processes that can affect their state. Whereas the substrate and biomass concentration fields are found by differential methods, tracking the biofilm development is done by discrete (CA) rules.

The *substrate concentration* in grid elements depends on the balance between transport mechanisms and reaction inside the biofilm. In the present model only the diffusive transport of substrate is considered for the cases studied: growth of colonies *in* the gel bead and for growth *on* a solid carrier. Therefore, only the reaction–diffusion equation must be solved in a 2D or 3D space to obtain the substrate concentration field.

In the general 3D system the mass balance for substrate is:

$$\frac{\partial c_S}{\partial t} = D_S \left(\frac{\partial^2 c_S}{\partial x^2} + \frac{\partial^2 c_S}{\partial y^2} + \frac{\partial^2 c_S}{\partial z^2} \right) - r_S(c_S, c_X) \qquad (1)$$

assuming only molecular diffusion and conversion of substrate, with the boundary conditions depending on system geometry and physics. The substrate conversion rate, r_s, depends on the substrate concentration, c_s, and biomass density in the biofilm, c_x. For biological processes, the rate, r_s, is usually defined as a Monod-like saturation function; for example, in the form given by Eq. (10).

For numerical reasons, it is better to use a partially dimensionless substrate balance. The variables are related to fixed quantities, preferably to the maximum value they can get: the space coordinates to the characteristic length (e.g., the bead diameter),

$$X = \frac{x}{d}, Y = \frac{y}{d}, Z = \frac{z}{d};$$

the substrate concentration to the concentration in the bulk liquid,

$$S = \frac{c_S}{c_{S0}};$$

and the biomass concentration to the maximum biomass density in a colony,

$$C = \frac{c_X}{c_{Xm}}.$$

There is no need to use a dimensionless time. Thus, with the new notations, the balance equation for substrate becomes:

$$\frac{\partial S}{\partial t} = \frac{D_S}{d^2}\left(\frac{\partial^2 S}{\partial X^2} + \frac{\partial^2 S}{\partial Y^2} + \frac{\partial^2 S}{\partial Z^2}\right) - \rho_S(C,S) \qquad (2)$$

where $\rho_S(C,S)$ is the normalized rate of substrate consumption. For example, using the particular Monod equation [Eq. (10)], the normalized rate of substrate consumption is $\rho_S(C,S) = r_S/c_{S0}$. The partial differential equations were solved numerically by finite difference relaxation algorithms (see Appendices).

The *biomass density* is computed by direct integration of the biomass balance equation, taking into account only growth of colonies as a result of substrate consumption. When the dimensionless biomass concentration in a grid cell reaches maximum value ($C_{x,y,z} = 1$), it will divide in two equal parts. The first one will stay on the same place, whereas the other will be placed somewhere in an adjacent grid element, ''pushing'' the neighbors according to a cellular automaton rule (see below).

Considering biomass accumulation to be the net result of biomass growth and biomass decay, the dimensionless biomass balance will be:

$$\frac{\partial C}{\partial t} = \rho_X(C,S) \qquad (3)$$

where $\rho_X(C,S)$ is the normalized rate of biomass accumulation. For the particular case discussed later, in which the rate, r_x, is given by a Monod with decay equation [Eq. (11)], $\rho_X(C,S) = r_X/c_{S0}$.

When this equation has no simple analytical solution, it can be solved using, for instance, a forward Euler step:

$$C^{(t+\delta t)} = C^{(t)} + \rho_X(C^{(t)},S^{(t)})\delta t_C \qquad (4)$$

to obtain the evolution of biomass concentration in every grid element.

The *occupation matrix,* **c,** is updated following a cellular automaton mechanism. The state of a site is marked as ''occupied with biomass'' ($c_{x,y,z} = 1$) when the corresponding biomass density is $C_{x,y,z} > 0$, as a result of the growth process. At the same time, other processes, such as attachment and detachment, can be simulated by appropriate rules that change the occupation state of the solids matrix, but they are not considered in the present study. The CA rule for growth is as follows:

If ($C_{x,y,z} \geq 1$) (*this means that the biomass density reached the maximum level in the elemental volume*)

1. The biomass in (x,y,z) is divided in two parts. The first stays at the same site, whereas the second part is counted as a new grid element containing biomass and must be placed in another space element.
2. A search for a free-space element is carried out among the nearest-neighbor elements.
3. **If** there are more free adjacent sites around [e.g., at least one $c_{x,y,z} = 0$, (x,y,z) being the coordinates of the four nearest neighbors]
   then put the new cell in one of them, randomly chosen with equal probability, and the search ends.
4. **If** there are no free sites for the new cell [e.g., all $c_{x,y,z} = 1$, (x,y,z) being the coordinates of the four nearest neighbors]
   then the new cell will displace a neighbor cell chosen at random.
5. The displaced cell will search again for a free-space element (cf. steps 2–4).

Biomass Detachment

To maintain the spherical geometry of the gel bead system, a mechanism for biomass detachment must be introduced. We adopted, in the 3D model, the most simple approach: if the space in which the newly formed biomass has to be placed is located outside the carrier sphere then the microorganisms are removed. Although the colony expulsion seems also to be a real mechanism of cells' detachment from the gel beads (Wijffels, 1994), only this ''single-cell release'' mechanism is considered here. In the future, more attention will be paid to detachment of biomass from biofilm structures.

Boundary Conditions

The substrate uptake from the environment is governed by a set of specific boundary conditions. For colonies expanding *in* a spherical bead (the particular case discussed in this article), the substrate concentration is maximal and constant outside the bead. If we neglect external mass transfer effects then the boundary condition is:

$$S = 1 = \text{constant (at any } t\text{)} \quad \text{for } r(x,y,z) = \sqrt{x^2 + y^2 + z^2} > R_{\text{bead}} \qquad (5)$$

If the external mass transfer resistance is important, the value of the substrate concentration surrounding the gel bead is computed as:

$$S = 1 - \frac{1}{Bi}\left.\frac{dS}{dX}\right|_{X=1} \text{ (at any } t\text{)} \quad \text{for } r(x,y,z) = \sqrt{x^2 + y^2 + z^2} > R_{\text{bead}} \qquad (6)$$

where the dimensionless parameter, $Bi = k_S d/D_S$, represents the ratio between the maximum substrate transfer rates outside and inside the bead. This type of boundary condition has been used in the 3D simulations.

Initial Conditions

The initial conditions, as well as the boundary conditions, are specific for the case studied. We will present here only the initial states of variables used in modeling the system in which cells are growing immobilized in gel beads (see Model Evaluation section).

Substrate

At time zero, substrate is at its maximum concentration and uniformly distributed in the space $S_{x,y,z}^{(t=0)} = 1$ for all (x,y,z) elements.

Biomass Density

A certain initial concentration of cells must be specified within the representative volume. How to distribute the biomass depends on the particular system geometry (and on the problem in question). Biomass can be uniformly distributed *throughout* a sphere of gel carrier and this case will be presented in this work. For development of a biofilm *on* a planar surface or on a sphere, microorganisms can randomly attach to the target surface; this application will be discussed in a forthcoming article.

Due to the fact that the number of volume elements (N^3 elements for cubic space or $N \times M \times L$ for any other rectangular space) is much higher than the initial number of bacteria introduced in the reference space, we can assume that there is only one bacterium in each element that becomes inoculated. Thus, the biomass density in each inoculated grid element is simply the ratio between the mass of a single bacteria (m_{cell}) and the volume of a grid element with the size, d/N,

$$\frac{m_{\text{cell}}}{V_{\text{elem}}} = m_{\text{cell}} \cdot \frac{N^3}{d^3}.$$

Then, the fraction of biomass from the maximum density will be:

$$f = \frac{m_{\text{cell}}}{c_{Xm}} \frac{N^3}{d^3} \tag{7}$$

where d is the dimension of the considered space (in the example in what follows, the diameter of gel sphere). Thus, the biomass content in each inoculum volume element is $C_{x,y,z}^{(t=0)} = f$.

Occupation State

Calculation of the initial number of volume elements inoculated begins with the assumption that the initial concentration of biomass in the gel is X_0 (kg biomass m^{-3} bead). Knowing the bead diameter, d, the mass of bacterial cells, m_b (kg biomass), introduced in one bead is:

$$m_b = \frac{\pi d^3}{6} X_0 \tag{8}$$

If the mass of one bacterial cell is m_{cell}, then the number of volume elements inoculated is:

$$n_0 = \frac{\pi d^3 X_0}{6 m_{\text{cell}}} \tag{9}$$

GENERAL PROCEDURE

The algorithm for microbial cells growing in a diffusional gradient of substrate is as follows:

- Initialization. *Seed the carrier surface or bead volume with microorganisms.* n_0 volume elements will be inoculated randomly with an amount of biomass f and the corresponding sites on the solids matrix will be marked as ''occupied.'' Specify also the initial substrate field.
- Step 1. *Find the substrate distribution at time* $t + \delta t_C$: $\mathbf{S}^{(t+\delta t_C)}$. The balance equation will be solved by an iterative algorithm (overrelaxation or the alternating-directions implicit method, see Appendices), starting with $\mathbf{S}^{(t)}$, until a quasi-steady state is reached (the concentration S at $t + \delta t_S$ converged). During this step, the matrices of biomass density, **C,** and occupation state, **c,** are unchanged. We can do this because the growth of biomass is very slow in comparison with substrate diffusion and consumption. The time step used for relaxation of **S** is $\delta t_S << \delta t_C$ (usually $\delta t_S < 1$ s and $\delta t_C = 1000$ s).
- Step 2. *Solve the biomass balance.* With the obtained $\mathbf{S}^{(t+\delta t_C)}$, the biomass growth rate is used in each grid element of $\mathbf{C}^{(t)}$ to calculate $\mathbf{C}^{(t+\delta t_C)}$. The biomass state of $t + \delta t_C$ can be found either by an analytical expression or by a numerical integration step.
- Step 3. *Redistribute the biomass according to the automaton rules.* Check each element that contains biomass to determine if the maximum density has been obtained ($C_{x,y,z}^{(t+\delta t_C)} \geq 1$). If yes, then biomass will be split in two equal parts and will be placed somewhere in space according to the discrete algorithm just presented. The occupation state matrix, **c,** will also be updated.

Then the algorithm goes back to step 1 to find the substrate distribution for the new state of biomass matrix, $\mathbf{C}^{(t+\delta t_C)}$. The evolution of this algorithm is presented in Figure 1.

MODEL EVALUATION

Immobilized Cells in Gels

Growth of immobilized cells has been studied extensively in recent years (Willaert and Baron, 1996). As growth proceeds in the gel, microcolonies expand until the surface of the beads is reached. At high initial biomass concentrations, many small microcolonies will be formed. After some time, colonies situated near the gel surface will become larger.

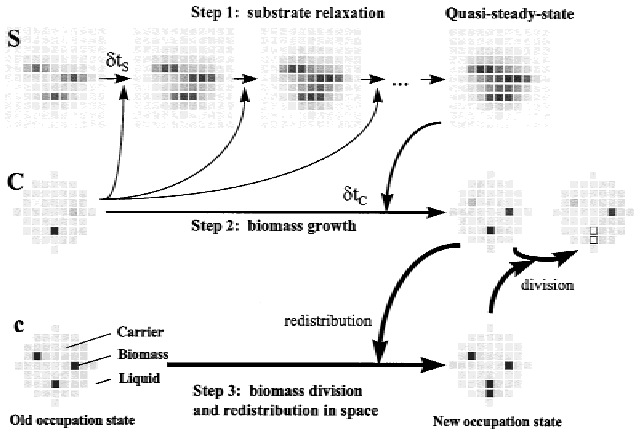

Figure 1. An example of computational steps used in one cycle by the algorithm of diffusion–reaction–growth. On substrate maps (S), the darker the gray nuance in a grid element, the lower the substrate concentration. On occupation maps (c), white means liquid, gray is the carrier, and black are spaces occupied by bacterial colonies. On biomass maps (C) the density in colonies varies from 0 to 1 and, accordingly, the color from white to black. The four substrate maps show the relaxation steps to a steady state (algorithm step 1). The substrate concentration in this steady state is then used to calculate the new biomass density in each grid element (step 2). In those elements where the critical biomass density has been reached, the biomass will be split and redistributed in space (step 3).

Finally, a compact biofilm layer will result at the surface of beads. If the initial biomass concentration is low, fewer but larger colonies will be formed (Wijffels et al., 1991a, b).

The case modeled here aims to validate the proposed combined differential–cellular automaton model, by showing a satisfying interpretation of recent experiments on nitrification with immobilized cells done by Wijffels et al. (1991a, b). Two kinds of data will be compared: nitrification with ammonia oxidizers (*Nitrosomonas europaea*) at different inoculum concentrations and nitrification with nitrite oxidizers (*Nitrobacter agilis*) at different dissolved oxygen concentrations. In both cases, oxygen is the limiting substrate.

It is important to establish what predicted quantities will be compared with the experimental results:

1. The evolution of *global oxygen consumption rate* will be the main quantitative validation point. The change in the consumption rate in time was determined for different dissolved oxygen concentrations and also at different biomass inoculum concentrations.
2. The *biomass distribution* in beads was measured and the results are compared with predictions of our model.
3. The *substrate concentration* profile in the bead was not measured by Wijffels et al. (1991a, b). Only in another experiment with biomass immobilized in agar layers was oxygen concentration measured with microelectrodes. Therefore, only a qualitative agreement between simulated profiles and measured ones is provided.

Parameters

We use the same parameters for microbial growth and diffusive O_2 transport as Wijffels et al. (1991a) did in the dynamic modeling of immobilized *Nitrosomonas europaea* (Table I, column a) and for *Nitrobacter agilis* (Table I, column b).

The rate of substrate (dissolved oxygen) consumption is (Beeftink et al., 1990; Wijffels et al., 1991a):

Table I. Parameters used in simulations: (a) variation of inoculum concentration (b) variation of dissolved oxygen in bulk liquid.

Parameter	Symbol	Value (a)	Value (b)	Units
Microorganism		*Nitrosomonas europaea*	*Nitrobacter agilis*	
Total number of volume elements	N^3	10^6	10^6	—
Initial concentration of biomass	X_0	$2 \cdot 10^{-3}$ and $2 \cdot 10^{-5}$	$4.5 \cdot 10^{-3}$	$kg_X\ m^{-3}$
Initial concentration of substrate	$c_{S,in}$	c_{S0}	c_{S0}	$kg_S\ m^{-3}$
Substrate in liquid volume	c_{S0}	$3.84 \cdot 10^{-3}$	$0.384 \cdot 10^{-3}$, $1.216 \cdot 10^{-3}$, and $2.56 \cdot 10^{-3}$	$kg_S\ m^{-3}$
Initial number of volume elements containing biomass [in 3D simulations, cf. Eq. (9)]	n_0	210 and 21,000	47,100	—
Fraction from the maximum biomass initially placed in inoculated elements [cf. Eq. (7) for $N = 100$]	f	$5.56 \cdot 10^{-4}$	$10.8 \cdot 10^{-4}$	—
Maximum specific growth rate	μ_m	$1.52 \cdot 10^{-5}$	$1.0 \cdot 10^{-5}$	s^{-1}
Growth yield from substrate	Y_{XS}	0.045	0.0362	$kg_X\ kg_S^{-1}$
Monod saturation constant	K_S	$3.5 \cdot 10^{-4}$	$3.75 \cdot 10^{-4}$	$kg_S\ m^{-3}$
Maintenance coefficient	m_S	$3 \cdot 10^{-5}$	$3.52 \cdot 10^{-5}$	$kg_S\ kg_X^{-1}\ s^{-1}$
Maximum biomass concentration	c_{Xm}	70	46	$kg_X\ m^{-3}$
Diffusion coefficient	D_S	$2 \cdot 10^{-9}$	$2 \cdot 10^{-9}$	$m^2\ s^{-1}$
Bead diameter	d	$2 \cdot 10^{-3}$	$2 \cdot 10^{-3}$	m
External mass transfer coefficient	k_S	$3.7 \cdot 10^{-5}$	$3.7 \cdot 10^{-5}$	$m\ s^{-1}$

$$r_S(c_S,c_X) = \left(\frac{\mu_m}{Y_{XS}} + m_S\right) c_X \frac{c_S}{K_S + c_S} \quad (10)$$

The net rate of biomass formation is:

$$r_X(c_S,c_X) = Y_{XS}(r_S(c_S,c_X) - m_S c_X) \quad (11)$$

The kinetic model used by Wijffels et al. (1991a) is a combination of the models of Pirt (1966) and Herbert (1959). Real biomass growth is governed by the specific growth rate, μ_m, and decay is included by the maintenance coefficient, m_S, and yield, Y_{XS}. At low substrate concentration (in the middle of the gel bead), this model will perform like the Herbert model, allowing negative net biomass growth. At high substrate concentrations (near to the bead surface) it acts like the Pirt model, reaching an observable maximum growth rate.

Table I also shows that one million volume elements are used and only a very small number of these are initially inoculated.

Validation of Numerical Methods

To check if the numerical method used for relaxation of the substrate field gives results accurate enough to be compared with experimental data, a series of computational tests was carried out. All the grid elements containing the spherical bead were, for this purpose, filled with biomass at different concentration levels: 0.7, 7, and 70 kg m^{-3}_{bead}. Then, the balance of substrate in steady state was solved by three different methods. Parameters were those from Table Ia, without external resistance to substrate transfer to the bead.

First, an orthogonal collocation method (Finlayson, 1972; Villadsen and Stewart, 1967) was used to solve the unidimensional balance of substrate (substrate concentration variable only along the radius). Because, for high biocatalyst densities, the consumption rates of substrate are very high, a very steep substrate profile would be obtained. Therefore, 25 collocation points were put in the range between 0 and 1, with a higher density between dimensionless radius 0.9 and 1. Results obtained by this method were used as reference, being very close to the exact solution of the differential equation. In the second method, for the same system, a two-dimensional substrate balance was solved to the steady state by the alternating directions implicit (ADI) method. The size of the square grid used here was 600 × 600 elements. The third test was done for the 3D model, using the ADI method above on a 120 × 120 × 120 grid.

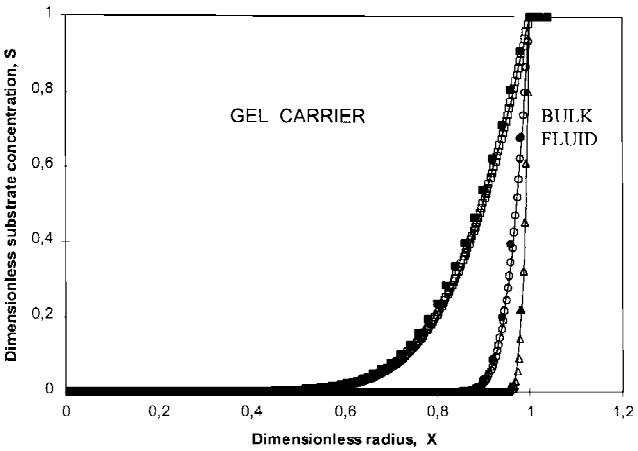

Figure 2. Comparison between calculated substrate profiles in the gel sphere at biomass concentrations of 0.7 (■ and □), 7 (● and ○), and 70 (▲ and △) kg m^{-3}, respectively. Filled symbols indicate points calculated with the 3D model (120 × 120 × 120); empty symbols are points calculated with the 2D model (600 × 600). Lines indicate interpolation between the solution of the unidimensional reaction–diffusion model at 25 collocation points.

For all three methods, the dimensionless substrate concentration was plotted against the dimensionless radius of bead. Concentration profiles for the three methods were obtained and were almost identical (Fig. 2).

Global oxygen consumption rates were computed from the obtained O_2 concentration profiles and the results presented in Table II. One can imagine more procedures to calculate the global rate (see Appendix 2); that is, using the average O_2 gradient at the bead surface and Fick's law (flux method), or using the integral of substrate consumption rates in each volume element (global method). It seems that, for high biomass densities, the rate cannot be well approximated by the flux method because of the very steep oxygen profile (a small change in slope at the surface of bead leads to big changes in rate values). Therefore, the global method was used when we compared experimental rates with those computed by the 3D model.

Two-Dimensional Model

A 2D grid can represent, for instance, a thin slice cut through the center of the bead. By neglecting colony ex-

Table II. Comparison of global oxygen consumption rates calculated by different methods (r_s in mol O_2 m^{-3}_{bead} s^{-1}).

Fraction from maximum biomass density, f	1D model (orthogonal collocation in 25 points)	2D model 600 × 600		3D model 120 × 120 × 120	
		Flux method	Global method	Flux method	Global method
1	0.0505	0.0426	0.0485	0.0280	0.0400
0.1	0.0153	0.0140	0.0158	0.0113	0.0133
0.01	0.0042	0.0039	0.0043	0.0035	0.0040

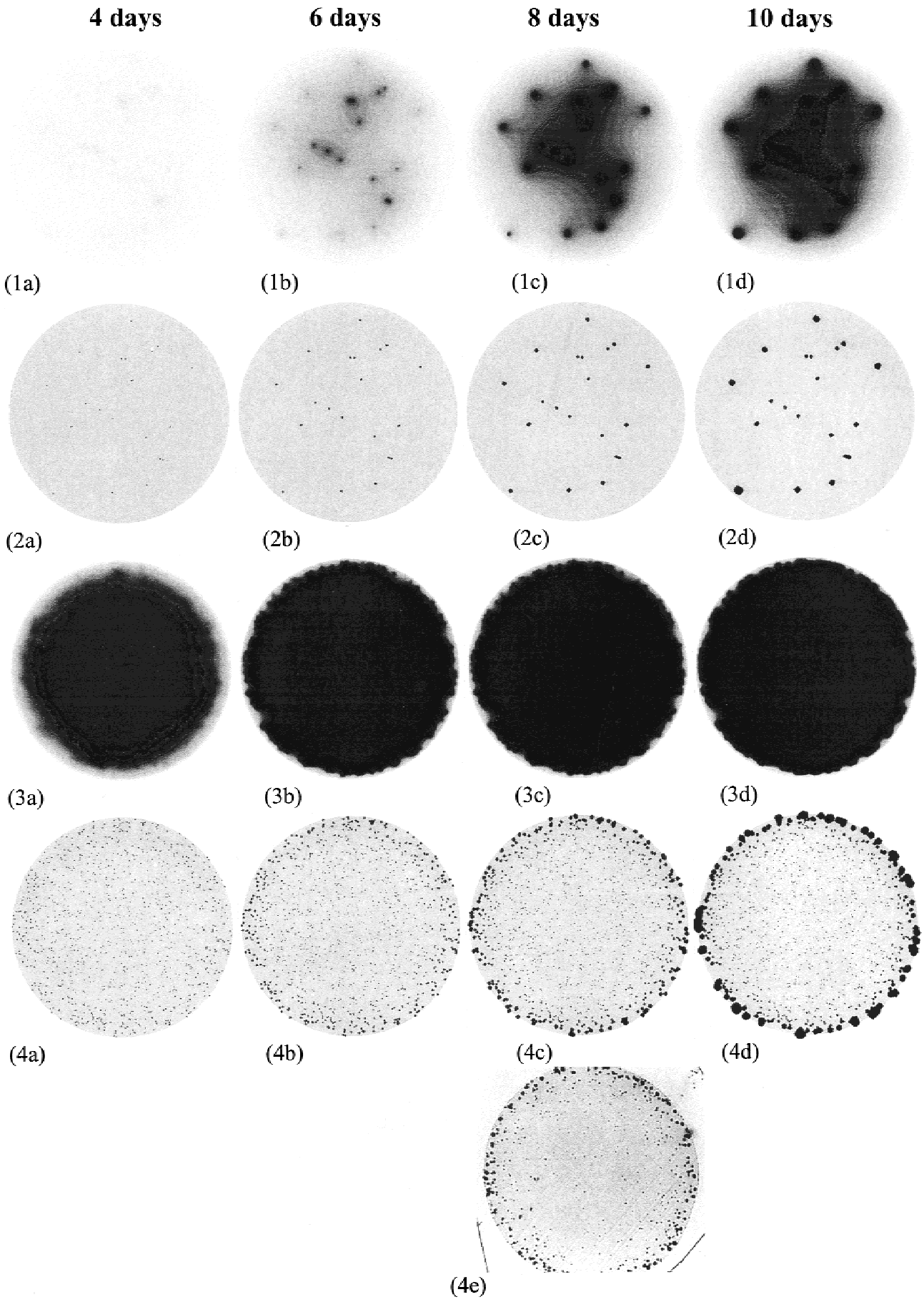

Figure 3. The spatial distribution of biomass and substrate in a 2D system with $N = 500$, $N_S = 250$ at $t = 4$, 6, 8, and 10 days (plots a–d, respectively). Substrate (1a–d) and biomass (2a–d) plots are for low inoculum density, $n_0 = 20$, whereas substrate (3a–d) and biomass (4a–d) maps are for high inoculum density, $n_0 = 1000$. Also note the striking resemblance of biomass map (4c) with (4e), picture of real colonies immobilized in the gel sphere (thin slice through the middle of the bead; see Wijffels [1994]). On substrate maps, the darker the gray area of a region, the lower the substrate concentration there. On biomass maps, white indicates liquid, gray indicates carrier, and black indicates spaces occupied by bacterial colonies.

pansion in a third dimension we would expect the model to predict larger colony diameters in 2D than observed in experiments. This is because the same amount of newly formed biomass must be distributed in a disk instead of a sphere. However, for the 2D case, substrate for growth is coming from only two directions, thus less substrate is available than in a 3D model. Therefore, the 2D model will be used only to obtain qualitative results and to demonstrate the differences from the 3D approach.

Our purpose was to study the dynamics of the reaction–diffusion–growth system for different initial biomass concentrations in the bead. For the 2D model, two hypothetical cases with $n_0 = 20$ and $n_0 = 1000$ grid elements initially inoculated in a 500×500 matrix will be presented here. All the other parameters are those from Table I (Column a), for nitrification with immobilized *Nitrosomonas europaea.*

The results of the 2D simulations are shown in Figure 3. On substrate maps, the darker the gray area of a region, the lower the substrate concentration there. On biomass maps, white means liquid, gray is the carrier, and black are spaces occupied by bacterial colonies. When the number of inoculated elements was low (e.g., 20 in Fig. 3.2a–d), then large colonies were obtained. Diffusional limitation in the gel did not play an important role in simulation times of less than 6 days (Fig. 3.1a–b). But, after 6 days, the lack of substrate in the middle of the bead (Fig. 3.1c–d) prevented colonies in the middle of the bead from growing further (Fig. 3.2c–d). Diffusional limitation of substrate into the colonies was significant after a certain colony size was reached.

In the case of dense initial distribution of biomass in the 2D grid (Figs. 3.3a–d and 3.4a–d), a differentiation in colonies size occurred from the early stages. Substrate diffusional uptake rate was low compared with its consumption in many colonies. As a result, colonies situated close to the surface grew faster and ultimately formed a dense bacterial layer. This phenomenon was experimentally observed by Wijffels et al. (1991a, b, 1994). A resemblance between the computed biomass map (Fig. 3.4c) and image of real colonies immobilized in the gel sphere, observed in a thin slice through the middle of the bead (Fig. 3.4e), is obvious. The corresponding average oxygen and biomass concentration profiles in the biocatalytical sphere, as they evolve in time, are shown in Figure 4.

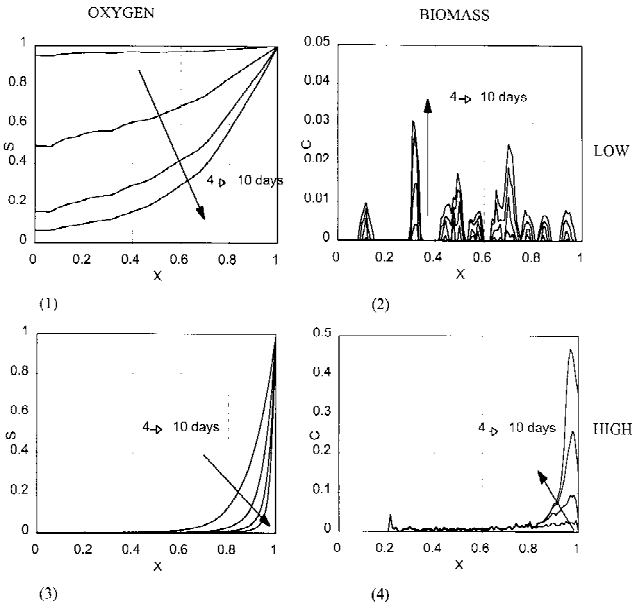

Figure 4. Average oxygen (1 and 3) and biomass (2 and 4) concentration profiles for low (1 and 2) and high (3 and 4) inoculation density. Graphs correspond to the 2D distributions presented in Figure 3, at $t = 4$, 6, 8, and 10 days.

Three-Dimensional Model

Why Three-Dimensional Modeling?

Calculations in a 2D system are of course easier; that is, one can work in a more refined grid and in a shorter computational time. Also, the same time average substrate and biomass profiles can be easily computed. However, when comparing the sizes of real biomass colonies with the 2D-simulated ones, differences appear. This is merely because representation of microbial growth in a flat space has a major drawback; that is, in reality, colonies expand in three dimensions. Working in a 2D space, the number of predicted colonies remains equal to the number of initial inoculum elements (death being neglected). However, in a 3D space, any 2D ''observation window'' will be periodically penetrated by colonies expanding from the third dimension.

This effect is clearly shown in Figure 5. After 5 days, four colonies appeared in a section made through the middle of the sphere (Fig. 5.1a). Corresponding, dark spots on the substrate distribution map could be seen (Fig. 5.2a). However, there were also other spots, indicating consumption of substrate by colonies in slices closer to or further from our observation slice. Indeed, after a certain time period, some of these neighboring colonies grew and appeared in the reference slice. In this way, the number of colonies counted continuously increased, an effect that cannot be represented in two dimensions.

Variation of Inoculum Concentration in Relation to Bead Performance

One of the most interesting experimental results obtained by Wijffels (1994) is that the initial biomass concentration in a gel carrier greatly affects the performance of the reactor. Starting with different inoculum concentrations we have seen that a gradient in colony sizes is obtained in 2D as well as 3D simulations (a continuous change from bigger colonies at the surface to smaller colony sizes at the middle of the gel bead).

Similar trends produced by the two-dimensional model were also observed in the 3D results. Colonies grown from a low initial concentration of microorganisms in gel (Fig. 5) were bigger than those grown starting with dense inocula-

tion (Fig. 6), which is because substrate is depleted faster in the latter case (Fig. 7a). Figures 5.1c and 5.3c show that, for low initial inoculum density, after a few days, larger colony sizes developed closer to the substrate source (the spherical boundary). For high inoculum density only the colonies situated near to the surface obtained substrate and they grew, forming a continuous bacterial layer (Fig. 6c).

The substrate concentration profiles in the gel agree qualitatively with those measured with an oxygen microsensor by Wijffels (1994) in agar slabs. Due to external mass transfer resistance, the substrate concentration at the surface decreased in time and the concentration gradient became steeper (biomass accumulation leads to higher consumption rates). In the case of low inoculation density, sub-

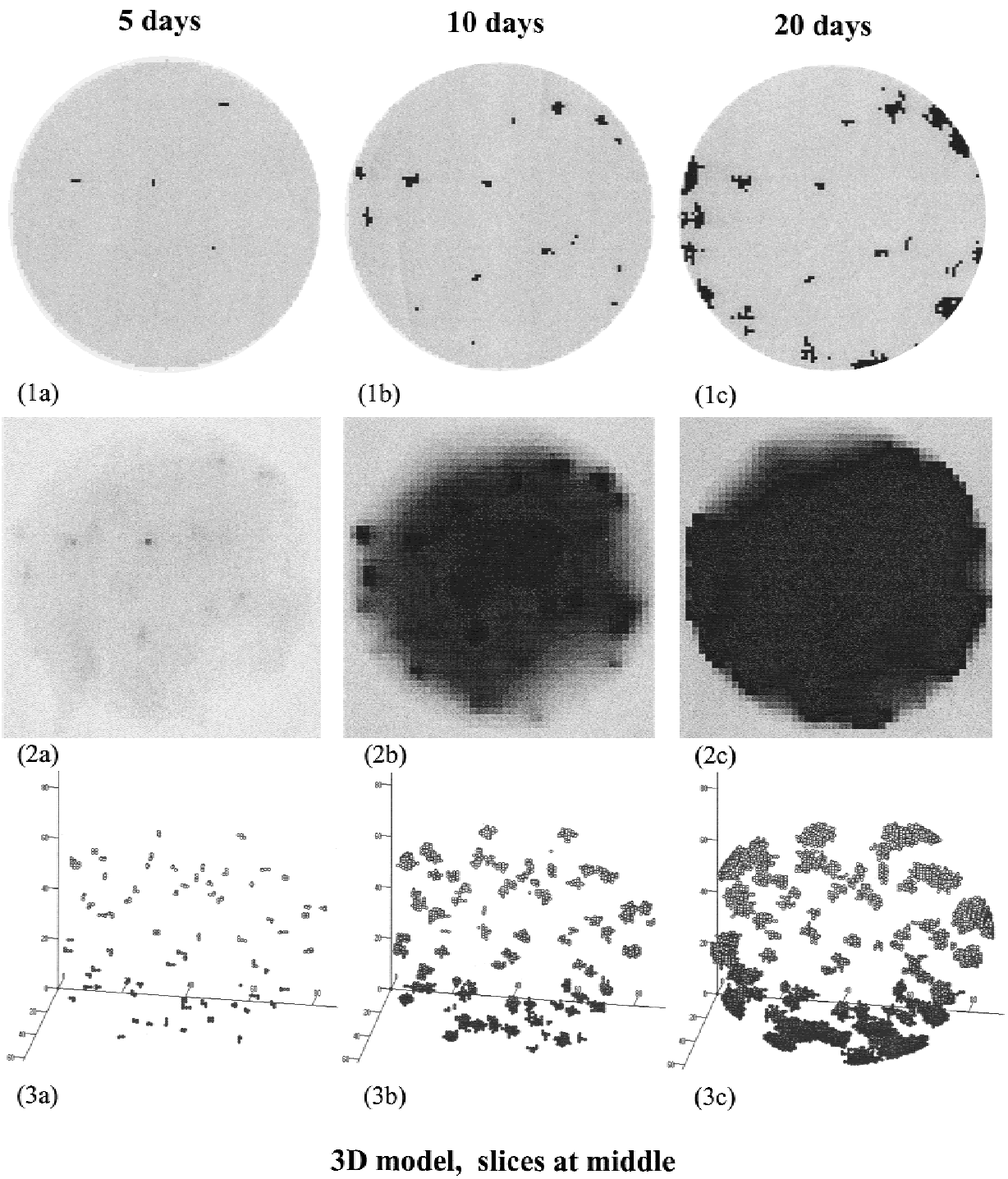

Figure 5. (1a–c) Maps of space occupation with biomass in a slice at the middle of the bead, over time. (2a–c) Maps of substrate distribution in a slice at the middle of the bead, over time. (3a–c) 3D plot of space occupation with biomass. The section is a median slice with a thickness of 40% of the bead diameter. This simulation was carried out with the 3D model using low inoculum concentration. Time: (a) 5 days; (b) 10 days; (c) 20 days. Significance of gray areas same as in Figure 3.

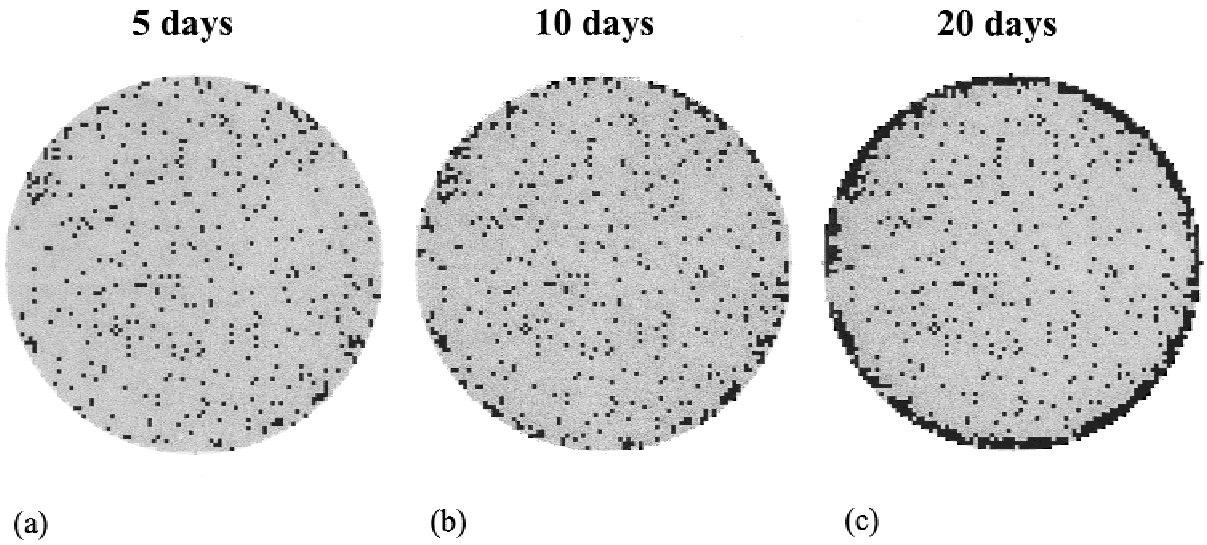

Figure 6. Maps of space occupation with biomass in the middle of the bead (3D model, high inoculum concentration). Time: (a) 5 days; (b) 10 days; (c) 20 days.

strate was still available in the center of the bead after 10 days (Fig. 7b), whereas, for high initial biomass concentration, it was completely depleted after only 5 days (Fig. 7a). This was also the moment when the global rate stopped its exponential growth (inflection point) and tended to be limited by the rate of diffusion (Fig. 9).

Although not as pronounced as for high inoculum concentration, the tendency to form more biomass near to the surface existed also for low inoculum at prolonged time periods (Fig. 5.3c and Fig. 8b). The ''sawtooth'' shape of the biomass profile toward the center of the bead was due to the higher uncertainty for averaging over a small number of volume elements.

Finally, we also compared the measured rates of substrate consumption (mol O_2 m_{bead}^{-3} s^{-1}) with the output of our model. In all 3D simulations, external mass transfer resistance was taken into account. All parameters (physical and biological) used in this simulation (Table I, column a) were those measured or selected from Wijffels (1994). The agreement between computer-simulated and measured consumption rates was good for high inoculation and poor for low inoculum concentration (Fig. 9). This is because, in the present model, we did not consider whole colony expulsion when the colony reached the surface of the bead (cf. Wijffels, 1994). If only single cells that expand out of the sphere are released into the liquid, a dense biomass layer would develop at the surface. This would lead to a much higher oxygen consumption rate than that observed in practice and would therefore explain the discrepancy in Figure 9.

Variation of Dissolved Oxygen Concentration in Relation to Oxygen Uptake Rate

One additional check was done comparing the macroscopic oxygen consumption rates of the immobilized nitrite-

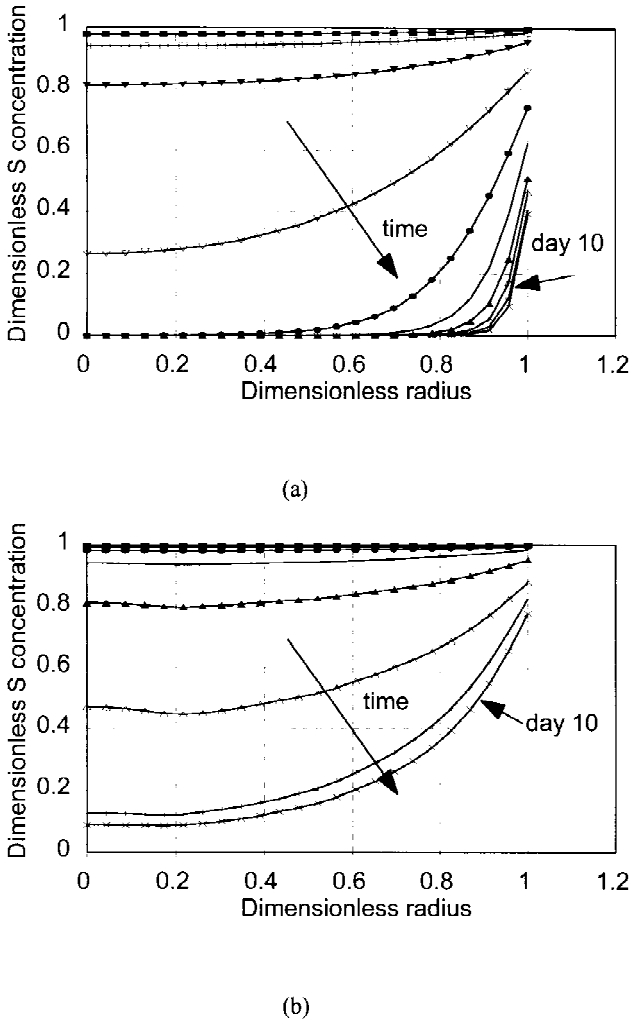

Figure 7. Calculated dimensionless substrate concentration profiles along the sphere radius, over time, from day 1 to day 10 (3D model). (a) High inoculum concentration; (b) low inoculum concentration. Symbols correspond to those in Figure 8.

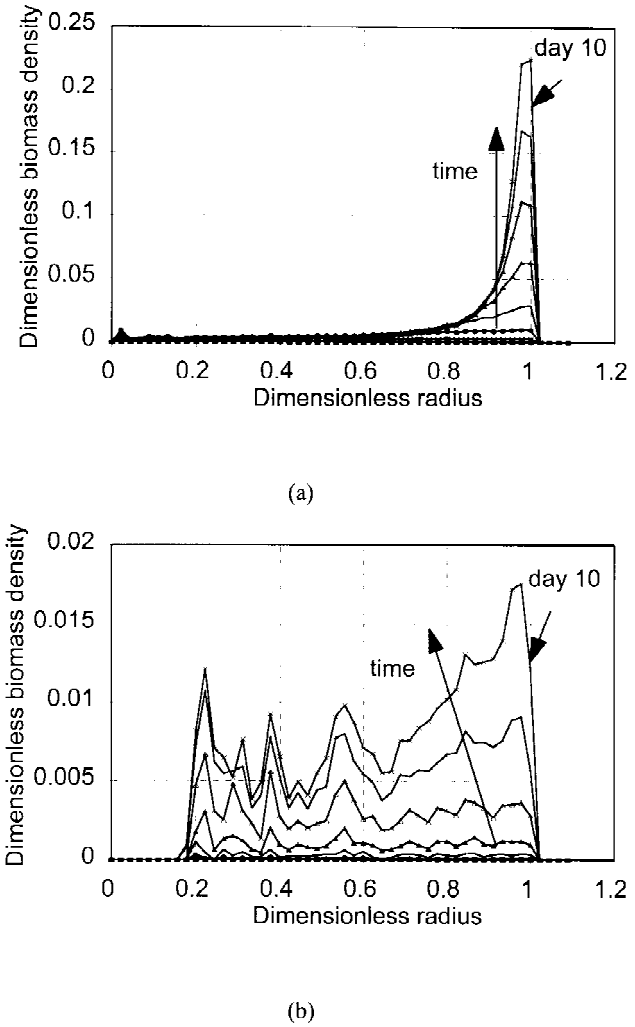

Figure 8. Calculated dimensionless biomass concentration profiles along the sphere radius, over time, from day 1 to day 10 (3D model). (a) High inoculum concentration; (b) low inoculum concentration. Symbols correspond to those in Figure 7. Note: the ordinate scale in (b) is 10 times smaller than in plot (a).

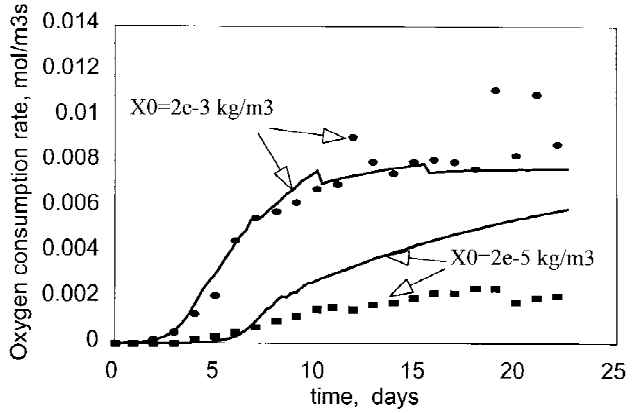

Figure 9. Evolution in time of the global oxygen consumption rate. Initial biomass concentration in the gel is $X_0 = 2 \cdot 10^{-3}$ and $2 \cdot 10^{-5}$ kg m^{-3} (markers ● and ■ for experimental data and lines for model results). The parameters used in this 3D simulation for growth of *Nitrosomonas europaea* immobilized in gel beads inoculated with different biomass concentrations are presented in Table I (column a).

oxidizing bacterium, *Nitrobacter agilis,* at three different oxygen concentrations in the liquid. The parameters used in the model are given in Table Ib (exactly the same as Wijffels et al. [1991a, b] used in their model evaluation).

As can be seen in Figure 10, there was a good agreement between experimentally measured rates and predicted ones for all three dissolved oxygen concentrations. This suggests once again that our approach was quantitatively correct and can adequately represent at least diffusion–reaction–growth systems.

DISCUSSION AND CONCLUSIONS

A new diffusion–reaction–growth model for immobilized microbial growth was developed. Although the spatial substrate distribution was assumed to be continuous and was found by solving conventional differential equations, the biomass spreading was modeled by a discrete cellular automaton algorithm. Newly formed biomass finds a place in space by ''pushing'' its neighbors to adjacent, unoccupied space. This is a new and more realistic feature, with other colony models having considered only growth of cells surrounded by free space (Hawboldt et al., 1994; Wimpenny and Colasanti, 1997; Zygourakis et al., 1991) or growth of motile bacteria that perform a random walk in neighboring space (Ben-Jacob et al., 1994; Schindler and Rataj, 1992). Moreover, these models are not quantitative.

Validation of the model was done for an immobilized cells system. Only diffusion-controlled growth and spread of colonies was considered. For the 3D model, a highly simplified mechanism for detachment of biomass spreading outside the gel carrier was also taken into account. Global oxygen uptake rates, concentration profiles for oxygen, and

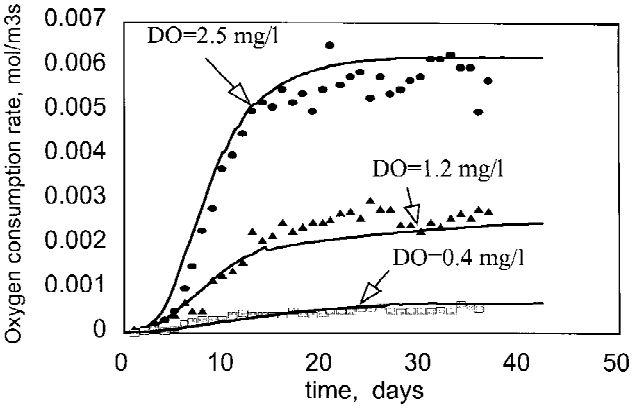

Figure 10. Evolution in time of the global oxygen consumption rate. Dissolved oxygen concentrations in bulk liquid are 0.4, 1.2, and 2.5 kg m^{-3} (markers ■, ▲, and ● for experimental data and lines for model results). The parameters used in this 3D simulation for growth of *Nitrobacter agilis* immobilized in gel beads are presented in Table I (column b).

biomass and colonies size were compared with those measured by Wijffels et al. (1991a, b) and Wijffels (1994). Results of calculations were both qualitatively and quantitatively in agreement with experimental data. Therefore, prediction of biomass and substrate distribution in two and three dimensions is now possible.

Two-dimensional representations use much less computational resources and can be easily implemented on ordinary personal computers. Therefore, the grid can be refined up to the bacterial level (~1 μm). However, 3D models give results comparable to experimental values. When properties such as porosity, density, or biofilm shape are the output of the model, only 3D models provide good results (forthcoming study). Thus, 3D models must be preferentially used for heterogeneous biofilm systems.

The proposed combined differential–discrete cellular automation approach is expected to be an excellent tool for study of biofilm development, because, using this approach, the geometrical shape and distribution of the biomass colonies, the porosity, and other structural parameters are predicted. In this respect, the approach is totally different from presently available models that need the biofilm geometry and porosity as input. One limitation of the model presented here is that it does not account for other processes that affect the biofilm morphology, such as attachment of solid particles, detachment of small or large biofilm patches, EPS production, or death of aged or starving colonies. Mathematical descriptions of these processes as a function of location in the biofilm still await experimentation.

APPENDIX 1: CALCULATION OF AVERAGE SUBSTRATE CONCENTRATION

Averaging of the substrate concentration, as well as the biomass density, was carried out on concentric rings (in 2D) and on concentric shells (in 3D) as follows:

$$S(r) = \frac{\sum_{i}^{N(r)} S_i(r)}{N(r)}, \quad \forall r = \sqrt{x^2 + y^2}\ for\ 2D\ or \quad \forall r = \sqrt{x^2 + y^2 + z^2}\ for\ 3D \tag{12}$$

where $N(r)$ is the number of grid elements in the ring with radius r.

APPENDIX 2: CALCULATION OF GLOBAL OXYGEN CONSUMPTION RATE

Flux Method

If the flux of substrate entering the bead is given by Fick's law, then the rate of substrate comsumption in one bead can be expressed as:

$$Q_{S,\text{bead}} = 4\pi R^2 \cdot D_S \left.\frac{dc_S}{dr}\right|_{r=R} \tag{13}$$

The number of beads in the reactor can be calculated from the solids fraction,

$$n_{beads} = \frac{V\varepsilon_S}{\frac{4}{3}\pi R^3},$$

so that the substrate consumption rate per reactor, Q_S (g O_2/s), will be:

$$Q_S = Q_{S,\text{bead}}\, n_{\text{beads}} = \frac{3}{R} V\varepsilon_S D_S \left.\frac{dc_S}{dr}\right|_{r=R} \tag{14}$$

And, finally, the global volumetric oxygen consumption rate, r_S (mol O_2 m_{gel}^{-3} s^{-1}), as a function of dimensionless concentrations and length ($S = c_S/c_{S0}$ and $X = r/d$), is:

$$r_S = \frac{3}{R}\frac{D_S}{M_S}\frac{c_{S0}}{2R}\left.\frac{dS}{dX}\right|_{X=1} \tag{15}$$

The concentration gradient at the surface of the bead can be approximated, knowing the average substrate concentration in concentric shells, $\bar{S}_i$ (with $i = 1 \ldots N_S/2$):

$$\left.\frac{dS}{dX}\right|_{X=1} \approx \frac{\bar{S}_{N_S/2} - \bar{S}_{N_S/2-1}}{\Delta X} \tag{16}$$

where $\Delta X = 1/N_S$ (N_S is the substrate grid dimension).

Thus, knowing the average substrate profile at a certain moment, we can calculate the macroscopic substrate consumption rate as:

$$r_S = \frac{3N_S}{2}\frac{D_S c_{S0}}{R^2 M_S}(\bar{S}_{N_S/2} - \bar{S}_{N_S/2-1}) \tag{17}$$

Global Average Method

The idea is to sum the rate contributions from all volume elements occupied with biomass. The rate of oxygen consumption in one element is $r_S(x,y,z)$ (kg O_2 m_{bead}^{-3} s^{-1}). Thus, the flow of oxygen consumed in one bead is:

$$Q_{S,\text{bead}} = \sum_{e\ \epsilon V_{bead}} r_S(x,y,z) \cdot V_e(x,y,z) \tag{18}$$

where e represents all elements with volume V_e situated at coordinates (x,y,z) in the bead.

Because all volume elements are identical and the number of beads in the reactor can be approximated, the substrate consumption rate per reactor, Q_S (kg O_2/s), is:

$$Q_S = \frac{V\varepsilon_S}{\frac{4}{3}\pi R^3} V_e \sum_{e\ \epsilon V_{\text{bead}}} r_S(x,y,z) \tag{19}$$

The rate of oxygen consumption per reactor volume will be (on molar basis):

$$r_S = \frac{1}{M_S}\frac{3}{4\pi R^3} V_e \sum_{e \in V_{bead}} r_S(x,y,z) \tag{20}$$

in which the volume of a grid element is $V_e = (d/N)^3$, and the reaction rate in the element as a function of dimensionless concentrations is:

$$r_S(x,y,z) = \left(\frac{\mu_m}{Y_{XS}} + m_S\right) c_{Xm} \cdot C_{x,y,z} \frac{S_{x,y,z}}{K_S/c_{S0} + S_{x,y,z}} \tag{21}$$

APPENDIX 3: NUMERICAL METHOD USED TO SOLVE SUBSTRATE CONCENTRATION FIELD

To solve the substrate field by a numerical method, Eq. (2) will be discretized according to a finite difference scheme. For simplicity, only the 2D case is discussed:

$$\frac{\delta_t S}{\delta t} = \frac{D_S}{d^2}\frac{\delta_x^2 S}{(\delta X)^2} + \frac{D_S}{d^2}\frac{\delta_y^2 S}{(\delta Y)^2} - \left(\frac{\mu_m}{Y_{XS}} + m_S\right)\frac{c_{Xm}}{c_{S0}} C \frac{S}{\frac{K_S}{c_{S0}} + S} \tag{22}$$

By grouping the terms, we rewrite the equation:

$$\delta_t S = (D_1\, \delta_x^2 S + D_2\, \delta_y^2 S - \rho_S(C,S))\delta t \tag{23}$$

where $\delta_t S = S^{(t+\delta t)} - S^{(t)}$, $\delta_x^2 S = S_{x+1,y} - 2S_{x,y} + S_{x-1,y}$, $\delta_y^2 S = S_{x,y+1} - 2S_{x,y} + S_{x,y-1}$, $D_1 = D_S/(d\delta X)^2$, $D_2 = D_S/(d\delta Y)^2$, and $\rho_S(C,S)$ is the substrate consumption term.

Several iterative schemes are described in the literature. In block iterative methods (Ames, 1977; Richtmyer and Morton, 1994), groups of components of $S^{(t+\delta t)}$ are modified simultaneously in such a way that we must solve a linear system for the whole subset of modified components at once. Therefore, individual components are defined *implicitly* in terms of other components of the same group. The blocks may be single rows (or columns) of the matrix, so that an algorithm is:

While $|S_{x,y}^{(t+\delta t)} - S_{x,y}^{(t)}| > admitted\_tolerance$

for each column $y \in [0, M]$

solve the tridiagonal system with $x \in [0, N]$:

$$a_1 S_{x+1,y}^{(t+\delta t)} + a_2 S_{x,y}^{(t+\delta t)} + a_3 S_{x-1,y}^{(t+\delta t)} = f(S_{x,y}^{(t)}; S_{x+1,y}^{(t)}; S_{x-1,y}^{(t)}; S_{x,y+1}^{(t)}; S_{x,y-1}^{(t)})$$

The *alternating direction implicit method* (ADI) for multidimensional heat flow and diffusion problems (Peaceman and Rachford, 1955), combines unconditional stability with calculational simplicity (Ames, 1977). For the 2D diffusion–reaction equation, two difference approximations on a square net are used alternatively on successive time steps of $\delta t/2$ each:

$$S^{(t+\delta t/2)} - S^{(t)} = D_1\frac{\delta t}{2}\delta_x^2 S^{(t+\delta t/2)} + D_2\frac{\delta t}{2}\delta_y^2 S^{(t)} - \rho_S(C^{(t)}, S^{(t)})\frac{\delta t}{2} \tag{24a}$$

$$S^{(t+\delta t)} - S^{(t+\delta t/2)} = D_1\frac{\delta t}{2}\delta_x^2 S^{(t+\delta t/2)} + D_2\frac{\delta t}{2}\delta_y^2 S^{(t+\delta t)} - \rho_S(C^{(t)}, S^{(t+\delta t/2)})\frac{\delta t}{2} \tag{24b}$$

where S stands for $S_{x,y}$. We use an iteration procedure. First, the initial set $S_{x,y}^{(0)}$ is selected. Having determined $S_{x,y}^{(t)}$ we then calculate $S_{x,y}^{(t+\delta t/2)}$ by a single row (line) iteration and then $S_{x,y}^{(t+\delta t)}$ by a single column iteration. Thus, to determine $S_{x,y}^{(t+\delta t/2)}$ from the first of these equations we must solve, for each value of y, a set of M simultaneous linear equations:

$$a_1 S_{x+1,y}^{(t+\delta t/2)} + a_2 S_{x,y}^{(t+\delta t/2)} + a_1 S_{x-1,y}^{(t+\delta t/2)} = b_1,\ x = 0...N-1 \tag{25}$$

where the coefficients and free term are:

$$a_1 = -1, \qquad a_2 = 2 + \frac{2}{D_1\delta t},$$
$$b_1 = \frac{D_2}{D_1} S_{x,y+1}^{(t)} + \left(\frac{2}{D_1\delta t} - 2\frac{D_2}{D_1}\right) S_{x,y}^{(t)} + \frac{D_2}{D_1} S_{x,y-1}^{(t)} - \frac{1}{D_1}\rho_S(C^{(t)}, S^{(t)})$$

The resulting matrix is tridiagonal, thereby allowing the application of a faster algorithm to solve the system of algebraic linear equations (the number of operations is proportional with N instead of N^3 as for straightforward Gaussian methods). Then, similar statements apply to the single column implicit part, and the system to be solved for each x is:

$$a_1 S_{x,y+1}^{(t+\delta t)} + a_2 S_{x,y}^{(t+\delta t)} + a_1 S_{x,y-1}^{(t+\delta t)} = b_2, \qquad y = 0 \ldots M-1 \tag{26}$$

We thank Dr. René Wijffels for permission to use his experimental data and images.

NOMENCLATURE

Bi	Biot number (–)
c_{S0}	substrate concentration in bulk liquid (kg oxygen m^{-3})
c_{Xm}	biomass maximum density in colonies (kg biomass m^{-3})
c_S, c_X	substrate and biomass concentrations in volume elements (kg m^{-3})
C	dimensionless biomass density (–)
d	bead diameter (m)
D_S	diffusion coefficient of substrate ($m^2\ s^{-1}$)
f	fraction of biomass from maximum biomass density in the colony (–)
K_S	Monod saturation constant for substrate (kg oxygen m^{-3})
k_S	external mass transfer coefficient (m s^{-1})
m_{cell}	dry mass of a bacterial cell (kg biomass)
m_S	maintenance coefficient (kg substrate kg^{-1} biomass s^{-1})
M_S	molecular weight of substrate (oxygen) (kg oxygen mol^{-1})
n_0	number of volume elements initially inoculated (–)
N, M, L	sizes of biomass and occupation state matrices (–)
N_S, M_S, L_S	sizes of substrate matrix (–)
r_S, r_X	substrate consumption and biomass formation rates (kg m^{-3} s^{-1})
R	gel bead radius (m)
S	dimensionless substrate concentration (–)

t	time (s)
X, Y, Z	dimensionless coordinates (–)
Y_{XS}	biomass yield from substrate (kg biomass/kg substrate)
X_0	initial biomass concentration in the gel (kg biomass m^{-3} gel)
x, y, z	spatial coordinates (m)

Greek symbols

δt_S	time step for substrate relaxation (s)
δt_C	time step for integration of biomass growth equation (s)
ρ_S, ρ_X	normalized rates of substrate consumption and biomass production (s^{-1})
μ_m	maximum specific growth rate (s^{-1})

Matrices

S	substrate matrix
C	biomass matrix
c	occupation state matrix

References

Ames, W. F. 1977. Numerical methods for partial differential equations, pp. 251–255. Thomas Nelson & Sons, UK.

Arvin, E., Harremoës, P. 1990. Concepts and models for biofilm reactor performance. Water Sci. Technol. **22**: 2177–2180.

Barker, G. C., Grimson, M. J. 1993. A cellular automaton model of microbial growth. Binary **5**: 132–137.

Beeftink, H. H., van der Heijden, R. T. J. M., Heijnen, J. J. 1990. Maintenance requirements: Energy supply from simultaneous endogenous respiration and substrate consumption. FEMS Microbiol. Ecol. **73**: 203–210.

Ben-Jacob, E., Schochet, O., Tenenbaum, A., Cohen, I., Czirók, A., Vicsek, T. 1994. Generic modelling of cooperative growth patterns in bacterial colonies. Nature **368**: 46–49.

Characklis, W. G., Marshall, K. C. 1989. Biofilms. John Wiley & Sons, New York.

Colasanti, R. L. 1992. Cellular automata models of microbial colonies. Binary **4**: 191–193.

Finlayson, B. A. 1972. The method of weighted residuals and variational principles. Academic Press, New York.

Fujikawa, H. 1994. Diversity of the growth patterns of *Bacillus subtilis* colonies on agar plates. FEMS Microbiol. Ecol. **13**: 159–168.

Gjaltema, A., Arts, P. A. M., van Loosdrecht, M. C. M., Kuenen, J. G., Heijnen, J. J. 1994. Heterogeneity of biofilms in rotating annular reactors: Occurrence, structure and consequences. Biotechnol. Bioeng. **44**: 194–204.

Hawboldt, K. A., Kalogerakis, N., Behie, L. A. 1994. A cellular automaton model for microcarrier cultures. Biotechnol. Bioeng. **43**: 90–100.

Herbert, D. 1959. Some principles of continuous culture, pp. 381–396. In: G. Tunevall (ed.), Recent progress in microbiology. Almqvist & Wiksell, Stockholm.

Laszlo, J., Silman, R. W. 1993. Cellular automata simulations of fungal growth on solid substrates. Biotechnol. Adv. **11**: 621–633.

Lim, J. H. F., Davies, G. A. 1990. A stochastic model to simulate the growth of anchorage dependent cells on flat surfaces. Biotechnol. Bioeng. **36**: 547–562.

Peaceman, D. W., Rachford, H. H., Jr. 1955. The numerical solution of parabolic and elliptic differential equations. J. Soc. Ind. Appl. Math. **3**: 28.

Pirt, S. J. 1965. The maintenance energy of bacteria in growing cultures. Proc. R. Soc. Lond. **163B**: 224–231.

Richtmyer, R. D., Morton, K. W. 1994. Difference methods for initial-value problems, pp. 211–217. John Wiley & Sons, New York.

Schindler, J., Rataj, T. 1992. Fractal geometry and growth models of a *Bacillus* colony. Binary **4**: 66–72.

Schindler, J., Rovensky, L. 1994. A model of intrinsic growth of a *Bacillus subtilis* colony. Binary **6**: 105–108.

Takács, I., Fleit, E. 1995. Modelling of the micromorphology of the activated sludge floc: Low DO, low F/M bulking. Water Sci. Technol. **31**: 235–243.

van Loosdrecht, M. C. M., Eikelboom, D., Gjaltema, A., Mulder, A., Tijhuis, L., Heijnen, J. J. 1995. Biofilm structures. Water Sci. Technol. **32**: 35–43.

Villadsen, J. V., Stewart, J. P. 1967. Solution of boundary-value problems by orthogonal collocation. Chem. Eng. Sci. **22**: 1483–1501.

Wanner, O., Gujer, W. 1986. A multispecies biofilm model. Biotechnol. Bioeng. **28**: 314–328.

Wanner, O., Reichert, P. 1996. Mathematical modeling of mixed-culture biofilms. Biotechnol. Bioeng. **49**: 172–184.

Wijffels, R. H. 1994. Pseudo-steady-state oxygen concentration profiles in an agar slab containing growing *Nitrobacter agilis:* Nitrification by immobilized cells, Ph.D. thesis, Wageningen Agricultural University, Wageningen, The Netherlands.

Wijffels, R. H., de Gooijer, C. D., Kortekaas, S., Tramper, J. 1991a. Growth and substrate consumption of *Nitrobacter agilis* cells immobilized in carrageenan: Part 1. Dynamic modeling. Biotechnol. Bioeng. **38**: 224–231.

Wijffels, R. H., de Gooijer, C. D., Kortekaas, S., Tramper, J. 1991b. Growth and substrate consumption of *Nitrobacter agilis* cells immobilized in carrageenan: Part 2. Model evaluation. Biotechnol. Bioeng. **38**: 232–240.

Willaert, R. G., Baron, G. V. 1996. Gel entrapment and microencapsulation: Methods, applications and engineering principles. Rev. Chem. Eng. **12**: 5.

Wimpenny, J. W. T., Colasanti, R. 1997. A unifying hypothesis for the structure of microbial biofilms based on cellular automaton models. FEMS Microb. Ecol. **22**: 1–16.

Zhang, T. C., Bishop, P. L. 1994a. Density, porosity and pore structure of biofilms. Water Res. **28**: 2267–2277.

Zhang, T. C., Bishop, P. L. 1994b. Evaluation of tortuosity factors and effective diffusivities in biofilms. Water Res. **28**: 2279–2287.

Zygourakis, K., Bizios, R., Markenscoff, P. 1991. Proliferation of anchorage-dependent contact-inhibited cells: I. Development of theoretical models based on cellular automata. Biotechnol. Bioeng. **38**: 459–470.